Soft Matter

Cite this: *Soft Matter*, 2011, **7**, 4179

www.rsc.org/softmatter

PAPER

Equilibrium chain exchange kinetics in block copolymer micelle solutions by dissipative particle dynamics simulations†

Zhenlong Li and Elena E. Dormidontova*

Received 8th December 2010, Accepted 10th February 2011
DOI: 10.1039/c0sm01443e

The kinetics of chain exchange between diblock copolymer micelles in solution at equilibrium were studied by dissipative particle dynamics simulation. We performed hybridization simulations for A_2B_3 or A_4B_x ($x = 4, 6, 8$) micelle solutions in which approximately half of all micelles and free chains were initially colored and chain exchange between micelles was monitored by analyzing the time-dependent fraction of colored chains in aggregates. We found that in all cases the chain exchange is dominated by chain (or small aggregate) expulsion and follows a first-order kinetic process with the characteristic time, τ, increasing exponentially with core block length, N_A and interaction parameter between blocks, χ_{AB} as $\tau \approx \exp(0.67\chi_{AB}N_A)$. We determined that chain exchange between micelles does not depend on concentration but occurs *via* several kinetic mechanisms: unimer expulsion/insertion, small aggregate fragmentation/merging and unequal size micelle fission/fusion, which all exhibit very similar relaxation times. Chain exchange between micelles in A_4B_x micelle solutions is found to occur more rapidly for diblock copolymers with a longer corona-block length, as the area per chain and critical micelle concentration are larger (while micelle size and critical micelle temperature are lower) in this case, implying a lower potential barrier for chain (or small aggregate) expulsion from micelles.

1. Introduction

In block copolymer micelle solutions at equilibrium polymer chains are constantly exchanging between different micelles. Understanding the chain exchange kinetics at equilibrium is of fundamental importance for directing polymer self-assembly and for different industrial applications of polymer micelles, such as in dispersant technology and controlled drug release.[1–3] There is a growing interest in this area as evidenced by a rapidly increasing number of publications. Despite a large body of data collected, a complete understanding of chain-exchange kinetics, especially the exchange mechanisms and the influence of different factors on chain exchange, is still lacking. In this paper we apply dissipative particle dynamics (DPD) simulations to study chain-exchange in micelle solutions of short diblock-copolymers with different polymer concentrations, interaction energies and corona-block lengths.

The chain exchange kinetics between block copolymer micelles in solution is most commonly explained based on a unimer expulsion/insertion mechanism.[4–6] According to this model, the chain exchange process is first order and yields a single-exponential decay function with a relaxation time (τ_{un}) determined by the potential barrier for unimer expulsion, which is concentration independent and occurs considerably slower than unimer insertion.[6] Unimer expulsion considerably slows down with an increase in the interfacial tension γ between blocks (or between core-block and solvent) and core-block length N_A: $\tau_{un} \approx \exp(N_A^{2/3}\gamma/kT)$ where k is the Boltzmann constant and T is temperature.[6] The dependence on corona-block length N_B comes only in a pre-exponential factor with τ_{un} increasing with N_B as a power-law function $\tau_{un} \approx N_B^{9/5}$, reflecting slower chain diffusion for longer corona blocks.[6,7] There are also other theoretical models suggesting that despite micelle fission/fusion being slower than unimer expulsion/insertion, it may also contribute to the chain exchange process.[7–10] Similar to unimer exchange, micelle fusion/fission slows down with an increase in incompatibility between blocks (or between core-block and solvent), core-block length and to less extent corona-block length. Micelle fusion/fission is expected to become more active with an increase of polymer concentration, as the probability of aggregate collision increases and the corresponding relaxation time τ_{mic} decreases with concentration. We note that theoretical approaches describing chain exchange kinetics in polymer micelles[6,7] consider the long chain(block) limit, *i.e.* $N_A \gg 1$, $N_B \gg 1$ and ignore the

Department of Macromolecular Science and Engineering, Case Western Reserve University, Cleveland, Ohio, USA 44106. E-mail: eed@case.edu

† Electronic supplementary information (ESI) available: Estimation of plateau level for contrast correlation function, unimer insertion correlation function, native chain expulsion by different mechanisms, effects of interaction energy and core block length on contrast correlation function, average surface area per chain and unimer fraction in solution for A_4B_4 and A_4B_8 micelle solutions. See DOI: 10.1039/c0sm01443e

often observed dependence of micelle aggregation number (size) on corona-block length.[11,12] The latter has to play a role in the kinetics of chain exchange between micelles, which will be discussed in this paper.

Various experimental techniques, such as nonradiative energy transfer and fluorescence-quenching techniques, sedimentation velocity, transmission electron microscopy, time-resolved light and small angle neutron scattering have been applied to study the process of chain exchange between equilibrium micelles in solution.[3,13–31] It has been found that the process of chain exchange between micelles can occur very quickly or slowly, depending on the system, with characteristic time scales that vary from milliseconds to days or even years for kinetically "frozen" solutions.[16,21,26] In micelle hybridization experiments designed to study chain exchange kinetics, typically block copolymers are labeled by fluorescent tags[14,17–20] or by hydrogen/deuterium (H/D) isotope substitution[25,29–31] and micelle solutions containing chains with one label are mixed with solution of very similar micelles carrying a different label. Chain exchange (hybridization) is detected by the time-dependent change in the fluorescence of the label molecules in the presence of each other or the scattering contrast of the micelles.[17–19,25,29–31] The chain-exchange kinetics are very sensitive to the properties of the micelle solution, such as the interaction between blocks (and/or solvent), temperature, chain length and system composition. The influence of interactions between the core- and corona-forming block or solvent has been studied by varying the solvent quality (by using co-solvent) or temperature.[17,20,23,25,28,29] It was found that a reduction of the solvent quality for the core or a temperature decrease can significantly slow down the chain exchange process or even leads to "frozen" micelles exhibiting no chain exchange in days or months.[16,26,29] In several cases an exponential dependence of the chain exchange relaxation time on the inverse temperature has been reported $\tau \approx \exp(E_a/kT)$, where E_a is a constant.[17,19,25] The influence of the core-forming block length N_A has also been studied and it was shown that an increase in N_A slows down the chain exchange process,[16,28] in qualitative agreement with theoretical predictions. The effect of the corona-forming block length N_B on chain exchange between micelles at equilibrium is more subtle and relatively few studies have addressed this problem. Underhill *et al.*[19] have found that an increase of the corona block length increases chain exchange between micelles, while Popelka *et al.*[28] report the opposite trend, *i.e.* a decrease in the chain exchange with an increase in N_B. In several micelle hybridization experiments the chain exchange rate was found to be independent of polymer concentration.[19,29,30] At the same time, often chain exchange can not be explained as a simple first-order process—a double-exponential fitting[17,19,23,25,32] or a more complicated process with a distribution of relaxation times leading to logarithmic decay[29–31] has been reported.

Monte Carlo and Stochastic Dynamics simulations have also been used to study chain exchange process between micelles at equilibrium.[33–37] Various auto-correlation functions were designed to characterize different relaxation processes, such as chain insertion, expulsion and chain exchange. Similar to experimental observations and theoretical predictions, the increase in insoluble block length and repulsive interaction energy between core- and corona-blocks (or solvent) has been shown to slow down the chain exchange in simulations[35,37] with an exponential dependence of the chain expulsion rate on inverse temperature reported for surfactant micelles.[36] The influence of polymer concentration was found to be more complex. The chain expulsion relaxation time was found to be independent of the polymer concentration, while the chain insertion relaxation time decreases with an increase of the polymer concentration.[33] The chain exchange process was shown to be dominated by the unimer expulsion mechanism at lower polymer concentration, while as the polymer concentration increases micelle fission/fusion starts to contribute more and more to the chain exchange due to the higher probability of micelle collision.[35]

Despite numerous studies devoted to chain exchange between micelles at equilibrium, there are still many questions remaining unanswered. For example, in what cases is a single-exponential decay function sufficient to describe the overall chain exchange kinetics? What is the contribution of different kinetic mechanisms (unimer insertion/expulsion, micelle fusion/fission) to the overall exchange process? What is the effect of different kinetics-controlling factors, such as the polymer concentration, interaction energy and block length, especially hydrophilic block length, on chain exchange as a whole and for each of the kinetic mechanisms? Aiming to answer some of these questions, in this paper we study the kinetics of chain exchange between micelles in solution using dissipative particle dynamics (DPD) simulations. DPD allows simulations on mesoscopic space and time scales, significantly exceeding the limits of molecular dynamic simulations while accurately addressing hydrodynamic interactions.[38,39] We performed *in silica* micelle hybridization experiments for A_2B_3 and A_4B_x ($x = 4, 6, 8$) micelle solutions (Fig. 1) at different polymer concentrations, interaction energies and corona-block lengths and analyzed the obtained results using different correlation functions. It has been demonstrated that DPD simulation can reproduce the scaling relationship for relaxation times and diffusion coefficients of polymers in both the melt and solutions with a chain length as short as 5.[40–42] DPD simulations have been successfully used to model the thermodynamics and kinetics of the process of surfactant and block copolymer micelle self-assembly,[43–46] indicating that DPD simulation is a very promising tool to study the chain exchange kinetics at the molecular level.

This paper is organized as follows. In the next section, we describe the details of our simulation approach and model. In the following section, we will present the results of hybridization simulations and discuss the influence of polymer concentration, interaction energy and corona block length on chain exchange kinetics using different correlation functions. Finally, we will summarize our findings in the Conclusions section.

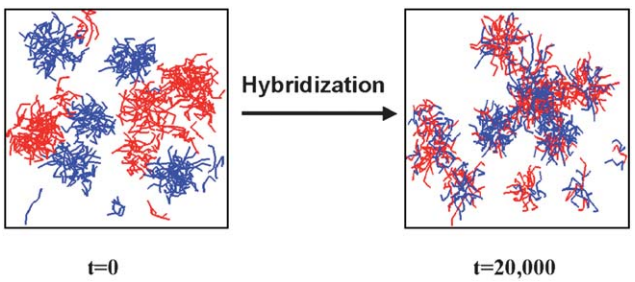

Fig. 1 Schematic representation of the micelle hybridization process.

2. Model and simulation details

To study the kinetics of micelle hybridization, we performed DPD simulations of dilute micelle solutions formed by short diblock copolymers (oligomers) upon self-assembly. In our simulations, a diblock copolymer (oligomer) was modeled as a coarse-grained linear bead-spring chain A_mB_x with m insoluble (A) beads and x soluble (B) beads linked by a harmonic bond force with a force constant $k = 100k_BT/d_p^2$ (k_B is the Boltzmann constant, T is temperature) and an equilibrium bond length $b_0 = d_p$, where d_p is the bead diameter. Solvent molecules were modeled as single beads identical to the soluble block bead (B) in a model chain. All beads in our simulations had the same mass m_0 and diameter d_p, which will be used as units of mass and length. All simulations were performed under periodic boundary conditions in a cubic box ($30d_p \times 30d_p \times 30d_p$) containing 81 000 beads. The density of all beads including polymer monomers and solvent was equal to $3d_p^{-3}$ and the repulsive interaction parameters between the same type of beads were $a_{AA} = a_{BB} = 25(k_BT/d_p^2)$, chosen to reproduce the compressibility of water at room temperature.[39] (In the following k_BT/d_p^2 will be omitted when referring to values of the interaction parameter a). Based on the value of the a_{BB} interaction parameter, the B-block is in a good solvent, as the chain length dependence of the radius of gyration and the diffusion coefficient for corresponding homopolymers follow scaling dependences with the Flory exponent of 0.6.[41,42] The cutoff distance for all DPD forces, including conservative force, dissipative force and random force[39] was the same $r_c = d_p$. The friction coefficient for the dissipative force was $3.0(k_BT/d_p^2)$ and the noise amplitude for the random force was $\sigma = (6)^{1/2}k_BT/d_p$.[39] In our simulations we considered two core-forming blocks $N_A = 2$ and $N_A = 4$. For micelle solutions of A_2B_3 chains, we varied the repulsive parameter ($a_{AB} = 47.5, 50, 52.5, 55$) and volume fraction of chains, φ (which is equal to concentration as d_p^3 is a unit volume), from 0.02 to 0.05 to study the interaction energy and oligomer concentration effects on the chain exchange kinetics. For solutions of A_4B_x chains, we kept the core block length ($N_A = 4$) and the volume fraction of chains ($\varphi = 0.05$) constant, and varied the soluble block length ($N_B = 4, 6, 8$) and repulsive parameter ($a_{AB} = 38, 40$) to study the chain length and interaction energy effects. Taking into account the relatively short chain lengths and low polymer concentrations considered, we will be exploring in this paper chain (and aggregate) diffusion in solution (corresponding to the Zimm regime) and in the micelle core (corresponding to the Rouse regime), both of which are well-reproduced using DPD.[40–42] In all simulations the NVT ensemble was adopted ($k_BT = 1$) and the equations of motion were integrated with a modified version of the velocity-Verlet algorithm[47] with time step $\Delta t = 0.04(m_0d_p^2/k_BT)^{1/2}$.[39] We used the free-source code LAMMPS[48] for the DPD simulations on the HPC computer cluster at Case Western Reserve University.

To obtain the equilibrium diblock copolymer micelle solution our DPD simulations were started from a random dispersion of model chains (obtained using $a_{ij} = 25$ for all pair interactions), and increased the interaction parameter a_{AB} to the desired value to initiate micelle self-assembly.[46] In the obtained equilibrium state aggregates were distinguished by a general distance criterion,[46,49] in which any pair of chains within a certain cut-off distance between the centers of mass of hydrophobic blocks belongs to the same aggregate. A cut-off distance of $1.2d_p$ was used to distinguish different aggregates for all systems with A_2B_3 chains, and a cut-off distance of $1.5d_p$ was used for aggregates composed of A_4B_x chains. The difference in cut-off distance reflects the size difference in the core-forming blocks. All equilibrated micelles had a spherical form. The simulations for equilibrated micelle solutions were conducted for $t = 3.2 \times 10^5$ for solutions with A_2B_3 chains and for $t = 1.2 \times 10^6$ for systems with A_4B_x chains. The movement trajectories were collected every 100 time steps for data analysis (discussed below). We used VMD[50] for displaying movement trajectories and data analysis. The equilibrium properties of the micelle solutions, including aggregation number distributions and micelle structure, have been discussed in our previous paper.[46] In Table 1, we summarize the equilibrium number-average aggregation numbers corresponding to the peak position of the aggregation number distributions and unimer volume fractions for the micelle solutions discussed in this study.

To study the chain exchange kinetics at equilibrium, we performed *in silica* micelle hybridization experiments (Fig. 1) inspired by previously reported experimental studies[29–31] using the movement trajectories generated from DPD simulations of equilibrium micelle state. In the *in silica* micelle hybridization experiment, at time $t = 0$ chains were randomly labeled blue in the largest aggregate and red in the next largest micelle until all chains in aggregates were marked and this initial configuration was accepted if the disparity between the total number of red and blue chains was less than 10%. Similarly, half of the unimers were labeled in red and other half in blue, so that the total number of red and blue chains was approximately equal to each other. As the time passes, chain exchange between micelles leads to a redistribution of red and blue chains between different micelles.

To evaluate the time-dependent progress of micelle hybridization, the following autocorrelation function $I(t)$ was used (*cf.* ref. 29 and 30):

$$I(t) = 4\left\langle \sum_N \left[\left(\frac{N_r(t)}{N(t)} - \frac{1}{2} \right)^2 \frac{N(t)}{N_{total}} \right] \right\rangle \quad (1)$$

where $N_r(t)$ and $N(t)$ are the number of red chains and the total number of chains in a micelle at time t and N_{total} denotes the total

Table 1 Equilibrium aggregation numbers determined from number-average aggregation number distributions M_{npeak} and unimer volume fractions φ_{unimer}, for A_2B_3, A_4B_4, A_4B_6, and A_4B_8 micellar solutions for different interaction parameters a_{AB} (the corresponding χ_{AB} values[39] are listed as well) at $\varphi = 0.05$

Oligomer	a_{AB}	χ_{AB}	M_n	φ_{unimer}[a] $\times 10^4$
A_2B_3	47.5	6.44	24 ± 7	19.0 ± 0.6
A_2B_3	50	7.15	31 ± 6	9.9 ± 0.5
A_2B_3	52.5	7.87	36 ± 6	4.9 ± 0.1
A_2B_3	55	8.58	43 ± 8	2.8 ± 0.4
A_4B_4	38	3.72	39 ± 10	15.8 ± 3.2
A_4B_6	38	3.72	26 ± 7	24.7 ± 3.5
A_4B_8	38	3.72	17 ± 4	32.6 ± 4.1
A_4B_4	40	4.29	51 ± 6	4.9 ± 2.9
A_4B_6	40	4.29	38 ± 4	8.9 ± 3.3
A_4B_8	40	4.29	31 ± 4	12.9 ± 4.3

[a] For all A_2B_3 micelle solutions φ_{unimer} was calculated for a given a_{AB} by averaging over different volume fractions, while for A_4B_x micelle solutions it was calculated by averaging over time.

number of chains in the solution. The summation is performed for all aggregates in the solution and $\langle \ldots \rangle$ denotes averaging over different initial states. $N_r(t)/N(t)$ represents the extent of hybridization for an individual micelle, while $N(t)/N_{total}$ is the weighting factor of the micelle, *i.e.* $I(t)$ is a weight average quantity, such as measured by a scattering experiment. At $t = 0$, there are no hybridized micelles (*i.e.* micelles containing both red and blue chains), $N_r(t)/N(t) = 1$ for red micelles and $N_r(t)/N(t) = 0$ for blue micelles, thus $4 \times (N_r(t)/N(t) - 1/2)^2 = 1$ for all micelles and $I(t)$ is practically 1. As hybridization proceeds, the fraction of blue and red chains in micelles becomes more equal and $I(t)$ decays with time, approaching 0 for the perfectly hybridized state (with exactly half red and half blue chains per aggregate). We note that due to the slight initial mismatch in the number of red and blue chains and some statistical effects of chain distribution between micelles (discussed below) the hybridization function $I(t)$ never reaches precisely zero.

3. Results and discussion

In this section, we present the results on chain exchange dynamics and discuss the effect of oligomer concentration, interaction energy, and corona block length.

Oligomer concentration effect for A_2B_3 micelle solutions

We have performed micelle hybridization simulations and calculated the autocorrelation function $I(t)$ using eqn (1) for A_2B_3 micelle solutions with different interaction energies and concentrations. Fig. 2 shows the hybridization curves $I(t)$ obtained at the same interaction energy ($a_{AB} = 50$) for different oligomer concentrations. As is seen, for all concentrations the initial slope of hybridization curves is rather similar and in all cases $I(t)$ decreases quickly, reaching different plateau levels at longer times. The plateau level originates from (a) the initial slight mismatch in the number of red and blue chains and (b) statistical deviations of the probability of finding a particular color chain in a given micelle from the average probability for the whole system (which decreases with an increase in the number of chains in the ensemble). These statistical effects are the main reason for the non-zero plateau level. Indeed, a random distribution of an equal number of red and blue chains among micelles results in the same (within simulation error) values of autocorrelation function eqn (1) as the plateau levels shown in Fig. 2 (see ESI†). To eliminate the influence of such statistical effects, which depend on the micelle size distribution, we normalized the autocorrelation function $I(t)$ and calculated the following contrast function (*cf.* experimental analysis[29–31]):

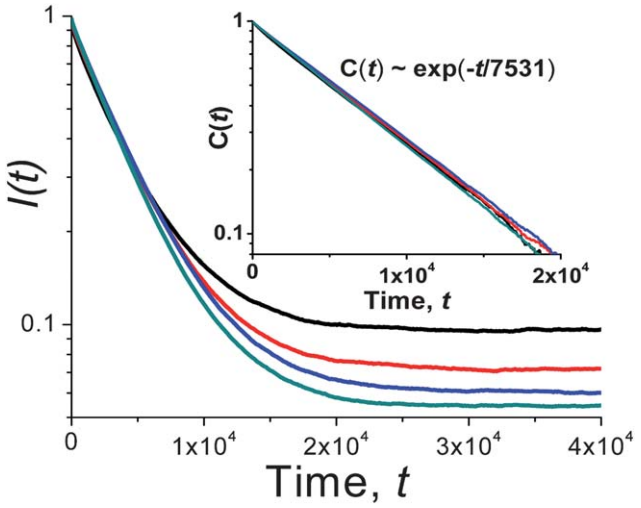

Fig. 2 Hybridization autocorrelation function, $I(t)$, eqn (1), and contrast function, $C(t)$, eqn (2) (inset) for A_2B_3 micelle solution with interaction energy $a_{AB} = 50$ at different oligomer concentrations: $\varphi =$ 0.02, 0.03, 0.04, and 0.05 (from top to bottom curves in the main plot, the color scheme is the same for the inset).

$$C(t) = \left[\frac{I(t) - I(\infty)}{I(0) - I(\infty)}\right]^{1/2} \quad (2)$$

where $I(\infty)$ is the plateau level, calculated by averaging $I(t)$ over the last $t = 1. \times 10^4$. We note that the contrast function is proportional to the average fraction of red (blue) chains in an average aggregate. By normalizing the original $I(t)$ curves shown in Fig. 2, we found that all contrast function $C(t)$ curves are practically the same, *i.e.* fall into a single line in a semi-log plot of Fig. 2 (inset). The obtained $C(t)$ dependence can be well-fitted by a single-exponential decay function with the corresponding characteristic relaxation time $\tau_c \approx 7.5 \times 10^3$. Similar analysis has been performed for A_2B_3 micelle solutions with different interaction energies for different concentrations and in all cases contrast functions $C(t)$ were found to be independent of concentration. The effect of interaction energy a_{AB} on the behavior of the contrast function $C(t)$ will be discussed in the next section. A singe-exponential decay of the contrast function indicates that there is one dominant relaxation process or there might be several processes with similar relaxation times that govern the chain exchange kinetics.

To understand which kinetic process or processes contribute to the chain exchange reflected in the contrast function (eqn (2) and Fig. 2), we first consider unimer expulsion/insertion, which is usually regarded as the dominant mechanism of chain exchange between block copolymer micelles at equilibrium.[6] Following ref. 36, we calculated the correlation function for unimer formation, $E(t)$. At time $t = 0$ chains in all aggregates were labeled. Whenever a labeled chain leaves a micelle and remains as a free chain for at least two consecutive time intervals, the chain was unlabeled. The time evolution of the number of labeled chains $N(t)$ was monitored and the ratio of $N(t)$ to the initial number of labeled chains $N(0)$ was calculated:

$$E(t) = \left\langle \frac{N(t)}{N(0)} \right\rangle \quad (3)$$

where $\langle \ldots \rangle$ denotes averaging over different initial states. Assuming that only unimer expulsion contributes to the formation of free chains in the solution, the correlation function $E(t)$ is expected to follow a single exponential decay and be concentration independent.[36] Fig. 3 shows in a semi-logarithmic plot the correlation function of unimer formation $E(t)$ for A_2B_3 micelle solutions with interaction energy $a_{AB} = 50$ calculated for different oligomer concentrations. As is seen, all curves indeed follow single-exponential decay, but there is an obvious dependence on oligomer concentration: unimer formation occurs slower for the micelle solutions with higher oligomer

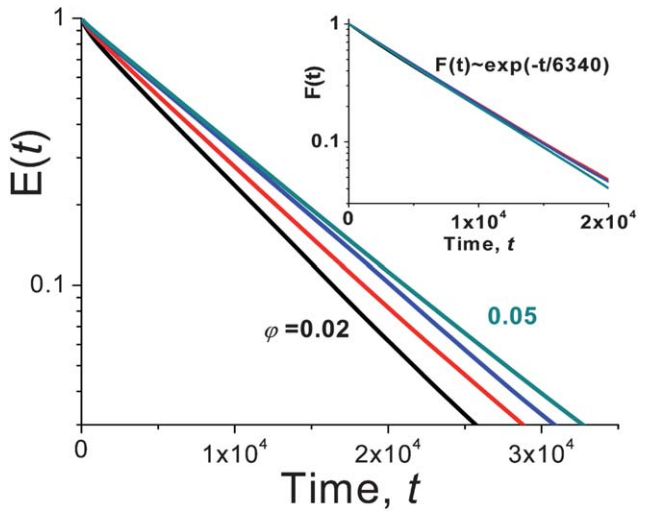

Fig. 3 Unimer formation, $E(t)$, eqn (3) and native chain expulsion, $F(t)$, eqn (4) (inset) correlation functions for A_2B_3 micelle solution with interaction energy $a_{AB} = 50$ for different oligomer concentrations ($\varphi = 0.02$, 0.03, 0.04, and 0.05, from bottom to top, the color scheme is the same for the inset).

concentration. A similar concentration dependence is also seen for A_2B_3 micelle solutions with different interaction energies (not shown).

By fitting the $E(t)$ curves in Fig. 3 with a single-exponential decay function ($f(t) = \exp(-t/\tau)$), we obtained the characteristic relaxation times for unimer formation, listed in Table 2. Comparing relaxation times for unimer formation, one can see a systematic increase of τ with an increase in oligomer volume fraction φ. As is seen from Table 2, the characteristic time for unimer formation is slightly smaller (for the lowest φ) or larger (for the higher φ) to that for contrast function $C(t)$. In general, the unimer insertion time (which decreases with concentration, see ESI†) is more than one order of magnitude smaller than unimer formation time, which implies that unimer escape is the rate-determining step for unimer exchange in agreement with analytical considerations.[6]

The observed concentration dependence of unimer formation function $E(t)$ (Fig. 3 and Table 2) indicates that in addition to direct unimer expulsion, there are other mechanisms which contribute to the unimer formation process. In particular micelle fusion/fission is known to be concentration dependent:

Table 2 Characteristic times obtained by a single-exponential decay fitting of contrast function (eqn (2)), unimer formation (eqn (3)) and native chain expulsion (eqn (4)) for A_2B_3 micelle solution with interaction energy $a_{AB} = 50$ at different oligomer concentrations

Contrast function,[a] $C(t)$	Unimer formation, $E(t)$	Native chain expulsion,[a] $F(t)$
0.02	6748	
0.03	7733	
0.047531 ± 214	8685	6340 ± 210
0.05	9032	

[a] The error-bars are obtained by averaging over corresponding different relaxation times obtained for different oligomer concentrations.

the higher the concentration the larger is the probability of these events. In the calculation of the unimer formation correlation function $E(t)$ a chain was unmarked only when it becomes a free chain regardless of its history. For instance, a marked chain could escape the initial micelle as a part of a small aggregate (*e.g.* a fission process) and be transported to another micelle before the chain finally escapes, become a free chain and be unmarked. To investigate the contribution of different mechanisms to the overall chain exchange process, we calculated the relative occurrence frequency as well as the overall contributions of different mechanisms including unimer expulsion/insertion, small aggregate (from dimers to tetramers) escape/formation and micelle (containing more than 5 chains) fission/fusion for A_2B_3 micelle solution (Table 3). A kinetic event was defined as the process of merging/splitting of two reactants (including unimers).[46] If the smallest aggregate contained 5 or more chains it was considered to contribute to micelle fission/fusion while if the smallest aggregate contained 2 to 4 chains this kinetic event was assigned to small aggregate fragmentation/merging (independently of the bigger reactant size). We note that the choice of the upper size boundary for small aggregates was dictated by the position of the minimum in micelle size distribution.[46] Any process involving unimers is categorized as unimer expulsion/insertion. The relative frequency is defined as the ratio of a number of events of a given type to the total number of events calculated averaging over the entire simulation and the contribution denotes the fraction of chains exchanged *via* the given kinetic mechanism compared to the total number of chains exchanged. As is shown in Table 3 for two oligomer concentrations, the unimer expulsion/insertion occurs more frequently (70%) than other two kinetic events, as expected. At the same time, the overall contribution of unimer exchange is about 30–40%, while the rest of the chains are exchanged *via* small aggregates expulsion/insertion or micelle fusion/fission. The contribution of unimer or small aggregate exchange decreases with an increase of concentration and the corresponding contribution of micelle fusion/fission increases (Table 3). As a result, the process of unimer formation considered in Fig. 3 is more likely to involve small aggregate exchange between micelles or micelle fission/fusion at higher oligomer concentration than at lower φ. Since such chain transport between the micelles directly contributes to the contrast function $C(t)$ but would delay the appearance of a free chain, the relaxation time for the correlation function $E(t)$ would increase with an increase of concentration, as is seen in Fig. 3 and Table 2.

To test the hypothesis that the observed concentration dependence for $E(t)$ correlation function for unimer formation originates from the contribution of other kinetic mechanisms besides direct unimer expulsion, we obtained correlation function for native chain fraction $F(t)$. At $t = 0$, all the chains in a given micelle (with the number of chains larger than 10) were marked as native chains, $N_{native}(0)$. The chain is unmarked if it leaves the micelle by any kinetic mechanism, either as a single chain or as part of an aggregate. During the simulation, the identity of the micelle during the time step t is traced as the micelle that contains more than half the chains compared to the preceding time step. The native chain correlation function $F(t)$ is calculated as:

Table 3 Relative frequency and contribution (fraction of chains exchanged) of different kinetic events, and corresponding relaxation times for native chain escaped by these mechanisms for A_2B_3 micelle solution with interaction energy $a_{AB} = 50$ at two different oligomer concentrations

	0.02			0.05		
Processes	Frequency (%)	Contribution (%)	Relaxation time, τ_{esc}	Frequency (%)	Contribution (%)	Relaxation time, τ_{esc}
Unimers	71 ± 1	40 ± 1	6154 ± 302	69 ± 1	30 ± 1	6021 ± 99
Small aggregates ($2 \leq P \leq 4$)	24 ± 2	33 ± 2	5964 ± 234	23 ± 1	24 ± 1	5829 ± 129
Micelles ($P \geq 5$)	5 ± 1	27 ± 1	5794 ± 67	8 ± 1	46 ± 1	6223 ± 75

$$F(t) = \left\langle \frac{N_{native}(0) - N_{leave}(t)}{N_{native}(0)} \right\rangle \quad (4)$$

where $N_{leave}(t)$ is the accumulating number of native chains that have left the micelle and the averaging occurs over different original micelles and different initial states. The native chain correlation function $F(t)$ is shown in the inset of Fig. 3 for A_2B_3 micelle solutions (with interaction energy $a_{AB} = 50$) for different oligomer concentrations. As is seen, all curves practically follow the same single exponential dependence with characteristic time $\tau_{esc} \approx 6340$, which is somewhat smaller than that for unimer formation or the contrast function $C(t)$ (Table 2). Comparing the unimer formation and native chain correlation functions, one can conclude that concentration dependence of the former is due to unimer transport between micelles by small aggregates or micelle fusion/fission processes, which become more active with a concentration increase. Another perhaps even more interesting conclusion, which can be made by comparing all three correlation functions (eqn (2), (3) and (4)) and the corresponding characteristic times (Table 2) is that a single exponential decay for the contrast and native chain correlation functions does not imply that chain exchange is dominated by a single kinetic process. Indeed, as is seen from Table 3 the contribution of small aggregate escape/insertion or micelle fusion/fission is comparable to that by unimer exchange for these short diblock copolymer micelle solutions. This implies that the characteristic times for unimer expulsion, small aggregate escape or even micelle fission should be comparable for this system to observe a single exponential dependence for the contrast and native chain correlation functions. To validate this point, we calculated the characteristic time for a native chain to be expelled from a micelle by three different mechanisms using eqn (4) for the native chain correlation function $F(t)$, in which $N_{leave}(t)$ is calculated as the accumulating number of native chains that have escaped the micelles by the corresponding mechanism and $N_{native}(0)$ is the total number of chains escaped by this kinetic mechanism. The obtained functions follow single-exponential decay (see ESI†) with characteristic relaxation times being very similar to each other, as is seen from Table 3. The physical origin for this behavior is a small difference in the energy barrier for a chain or a group of chains to leave a micelle due to a short length of the core-forming block, as discussed below.

Interaction energy effect

The interaction energy between blocks or between core block and solvent plays an important role in thermodynamics and kinetics of micelle self-assembly. We have performed micelle hybridization simulations for A_2B_3 micelle solutions with different interaction energies a_{AB} at different oligomer concentrations. As discussed in the previous section, oligomer concentration does not influence the obtained contrast correlation functions $C(t)$ (eqn (2)). The interaction energy has very strong effect, as is seen from Fig. 4, where contrast functions are shown for A_2B_3 micelle solutions with different interaction energies a_{AB}. All curves follow a single exponential decay. With an increase in a_{AB} the exchange of chains between micelles considerably slows down and the characteristic time increases (see ESI†).

The increase in the interaction energy leads to a higher surface tension at the core–corona interface which increases the aggregation number, decreases the critical micelle concentration (cmc) (and hence unimer volume fraction as listed in Table 1) and increases the potential barrier for chain expulsion (and aggregate escape or micelle fission).[6,7] Indeed, the free energy barrier for a block copolymer with a short core block N_A to escape from a micelle is defined primarily by the volume interaction energy of the block in solution:[51,52]

$$\tau_{un} \approx \exp(c\chi_{AB}N_A) \quad (5)$$

where χ_{AB} is the Flory–Huggins interaction parameter between monomers A and B and c is coefficient close to unity.[51,52] As has been shown in ref. 39, in DPD simulations the interaction energy parameter a_{AB} can be related to the Flory–Huggins interaction parameter χ_{AB}, as

$$\chi_{AB} = 0.286\Delta a_{AB} = 0.286(a_{AB} - a_{BB}) \quad (6)$$

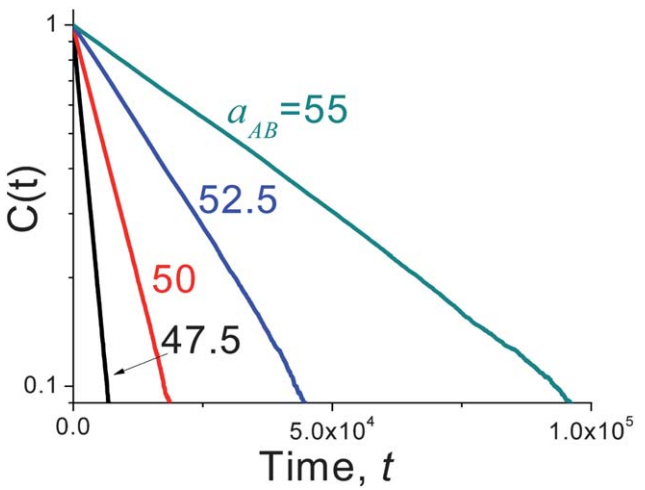

Fig. 4 Contrast function, $C(t)$, eqn (2), obtained for A_2B_3 micelle solutions with different interaction energies ($a_{AB} = 47.5$, 50, 52.5, and 55) at the oligomer concentration $\varphi = 0.03$.

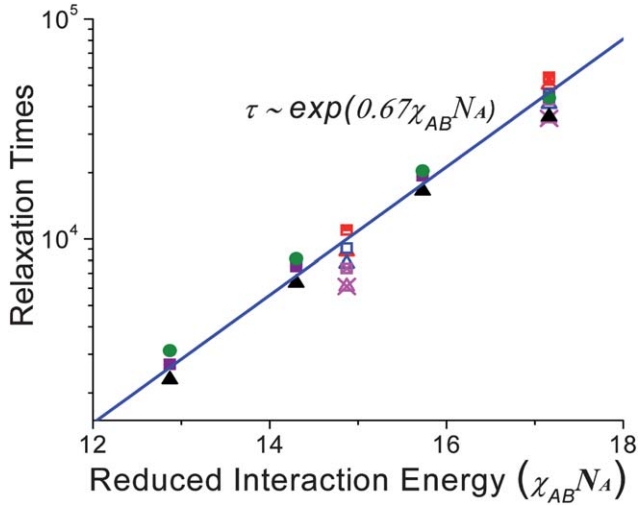

Fig. 5 Characteristic times for contrast $C(t)$ (eqn (2), squares), unimer formation $E(t)$ (eqn (3), circles) and native chain expulsion $F(t)$ (eqn (4), triangles) correlation functions for A_2B_3 micellar solutions at $\varphi = 0.03$ (filled symbols), and A_4B_4 (half-filled symbols), A_4B_6 (open symbols), A_4B_8 (crossed symbols) micelle solutions at $\varphi = 0.05$ as functions of reduced interaction energy $\chi_{AB}N_A = 0.286N_A\Delta a_{AB} = 0.286N_A(a_{AB} - a_{BB})$.

where $\Delta a_{AB} = a_{AB} - a_{BB}$. To investigate whether the relationship displayed in eqn (5) holds for the characteristic time for chain exchange obtained from hybridization simulations (Fig. 4) we plotted the corresponding data in Fig. 5 as a function of reduced interaction energy $\chi_{AB}N_A = 0.286N_A\Delta a_{AB}$. As is seen, the data follow linear dependence in the semi-logarithmic scale of the figure in agreement with eqn (5). We have also performed simulations and data analysis for native chain expulsion correlation function $F(t)$ (eqn (4)) for A_2B_3 and A_4B_x micelle solutions with different interaction energies and unimer formation correlation function $E(t)$ (eqn (3)) for A_2B_3 micelle solutions. The obtained characteristic times follow very similar dependence on reduced interaction energy $\chi_{AB}N_A$ (Fig. 5) and were fitted together with the characteristic times for corresponding contrast functions $C(t)$, leading to $\tau \approx \exp(0.67\chi_{AB}N_A)$. Thus, the obtained characteristic times for different correlation functions for both A_2B_3 and A_4B_x micelle solutions closely follow the dependence of eqn (5) that indicates that the energy barrier for chain escape or exchange is primarily defined by volume interactions between the core block and solvent (or corona block). We note that in the limit of high values of χ_{AB} (*i.e.* large values of Δa_{AB}) the relation described by eqn (5) may no longer be valid as aggregate formation can become kinetically controlled or aggregates may have a different equilibrium morphology (*e.g.* cylinders). As will be discussed below, there is an additional effect of corona block length N_B on chain exchange kinetics (which is responsible for some spreading of the data for A_4B_x micelle solutions in Fig. 5).

As discussed in the preceding section, the characteristic times for different correlation functions for A_2B_3 micelle solutions are not associated with a single kinetic process such as unimer escape/exchange, but rather a reflection of several processes such as small aggregate escape/insertion or even micelle fusion/fission occurring at comparable time scales. For unimer escape with the short core block as considered in our simulation study, the potential barrier is defined by volume interactions experienced by each A-type monomer surrounded by B-monomers, as described by eqn (5). For a small aggregate that has escaped from a micelle, core-block monomers will be able to reduce volume interaction to surface interactions with corona blocks or solvent solution,[6,7] which will reduce the corresponding potential barrier. Thus, for an aggregate of 10 or fewer monomers (which is the typical size of aggregates exchanged between A_2B_3 micelles even for micelle fission/fusion events) the potential barrier for small aggregate escape/exchange will be very comparable with that for single chain escape (eqn (5)). We note that for much longer core-forming blocks we would expect that the analytical prediction[6] for the potential barrier for unimer escape $\tau_{un} \approx \exp(N_A^{2/3}\gamma/kT)$ will be recovered, as the core block is expected to assume a more compact conformation in solution. In such a case the difference in potential barriers for unimer (or small aggregate) escape and micelle fusion/fission will become greater. It will be interesting to see whether this trend can be observed in computer simulations of longer polymer chains, which we hope to perform in the future.

Corona block length effect

As discussed in the previous section, the potential barrier for chain exchange follows the dependence of eqn (5), which implies that chain exchange considerably slows down with an increase in interaction energy a_{AB} or core-block length, N_A. The influence of the corona block length N_B on the chain exchange dynamics is normally considered to be a rather minor factor (at least in the limit of large N_B) and is primarily associated with the slower chain diffusion for a longer corona blocks.[6,7] We have performed hybridization simulations and calculated the contrast function (eqn (2)) for A_4B_x micelle solutions with different corona block lengths, which is shown in Fig. 6 for $a_{AB} = 38$. As is seen, an increase in the corona block length leads to a quicker chain exchange for micelle solutions with the same core block. The same trend is observed for interaction energy $a_{AB} = 40$ (see ESI†).

We have also calculated for A_4B_x micellar solutions the native chain expulsion (eqn (4)) correlation functions and observed very

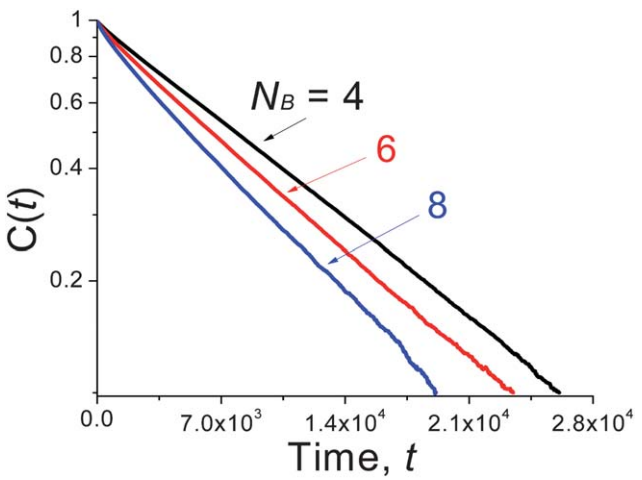

Fig. 6 Contrast correlation function $C(t)$ (eqn (2)) for A_4B_x micelle solutions with different corona block lengths ($N_B = 4, 6, 8$) for $a_{AB} = 38$, $\varphi = 0.05$.

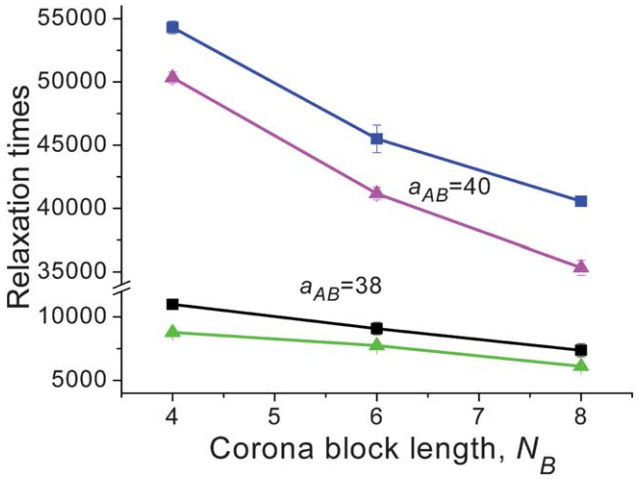

Fig. 7 Characteristic times for contrast $C(t)$ (eqn (2), squares) and native chain expulsion $F(t)$ (eqn (4), triangles) correlation functions for A_4B_4, A_4B_6 and A_4B_8 micelle solutions with different interaction energies at $\varphi = 0.05$ as functions of corona block length N_B.

similar dependence on the corona-block length N_B as for the contrast function (see ESI† and Fig. 7). As is seen from Fig. 7, the characteristic times for both correlation functions systematically decrease with an increase in corona block length implying that in all cases chain exchange becomes quicker with an increase in N_B. The obtained results indicate that there are other more important factors than decreasing the diffusion coefficient with an increase of corona-block length, which result in a quicker overall chain exchange in our A_4B_x micelle solutions. Similar to A_2B_3 micelle solutions, the characteristic time scale for unimer insertion into a micelle is one or even two orders of magnitude smaller than chain expulsion time for A_4B_x micelle solutions, and therefore this is not a factor determining the chain exchange rate.

As it has been shown in experimental, simulation and analytical studies, the increase in the corona-block length (for a given core-forming block) leads to a decrease of the average micelle aggregation number,[11,12,45,53,54] and perhaps more importantly increases the critical micelle concentration (cmc).[54–59] The main reason is that by having a longer soluble block a diblock copolymer has higher compatibility with solvent and a somewhat weaker tendency to form micelles compared to a diblock with shorter soluble block (and the same core block). We note that this effect will be especially noticeable for diblocks with a small mismatch between the core and corona block lengths and shorter overall chain length, as considered in our simulations. Indeed, as is seen from Table 1, the increase in B-block length results in a considerable decrease in the micelle aggregation number and an increase in unimer concentration. Furthermore, the area per chain in the micelle corresponding to the most probable aggregation number increases with an increase in the corona-block length (see ESI†), making it easier for a chain to escape from a micelle. Besides an increase in the cmc for diblocks with a longer soluble block, there is also a decrease in the cmt (critical micelle temperature). Indeed, comparing the unimer fraction (*i.e.* the fraction of free chains to the total number of chains) for different corona-block lengths, we observe that unimer fraction for A_4B_8 micelle solution significantly increases with a decrease in Δa_{AB} (which is linearly proportional to χ_{AB}, eqn (6) and hence inversely proportional to temperature) and remains consistently higher than that for A_4B_4 case (see ESI†). Having a higher cmc and lower cmt for micelles formed by diblock copolymers with longer corona-block length indicates that there is a higher penalty for chain transfer from the bulk to a micelle and therefore a lower potential barrier for a chain escape from the micelle,[13,60] which translates into more rapid chain exchange kinetics as shown in Fig. 6 and 7. In terms of the influence of corona-block length on the chain exchange mechanisms, an increase in B-block length leads to the decrease in frequency and contribution of micelle fission/fusion (since a thicker corona makes it more difficult for the cores of two micelles to come into contact) and an increase in the contribution of unimer exchange and small aggregate escape/insertion (see ESI†).

4. Conclusions

In this paper we have studied the kinetics of chain exchange between diblock copolymer micelles in solution at equilibrium using DPD simulations. In our *in silica* micelle hybridization experiments (Fig. 1) inspired by previously reported experimental studies, approximately half the micelles and chains were randomly labeled red and another half blue and chain exchange between micelles has been observed and analyzed in terms of the contrast function (eqn (2)). To gain insights on the process of chain exchange at the molecular level we also obtained correlation functions for unimer formation (starting from marked chains located in micelles, eqn (3)) and native chain escape (eqn (4)). We found that for all micelle solutions studied all correlation functions follow a single exponential decay. The corresponding relaxation times for the contrast function, unimer formation and native chain correlation functions were found to follow an exponential dependence on the interaction energy χ_{AB} (which is related to the difference in the interaction parameters $a_{AB} - a_{BB}$ according to eqn (6)) and core block length N_A: $\tau \approx \exp(0.67\chi_{AB}N_A)$. The decrease in chain exchange rate with an increase in core block length and incompatibility between blocks (or between the core block and solvent) is a result of a higher potential barrier for chain (or small aggregate) expulsion.[6,7] For short core blocks as considered in our simulation study, the potential barrier is defined by volume interactions experienced by each A-type monomer in the surroundings of B-monomers, $\sim\chi_{AB}N_A$. For a small aggregate core-block monomers will be able to reduce volume interactions to surface interactions with corona blocks or solvent in solution which will define the corresponding potential barrier $\sim N_A^{2/3}\gamma/kT$.[6,7] Thus, for an aggregate of 10 or less monomers (which is the typical size of aggregates exchanged between A_2B_3 micelles even for micelle fission/fusion events) the potential barrier for small aggregate escape/exchange will be very comparable to that for single chain escape, as shown in Table 3. As a result, despite the fact that there is more than one kinetic mechanism that contributes to chain exchange, as is seen from Fig. 3 and Table 3 (*e.g.* unimer expulsion/insertion only accounts for about 30% of the total number of exchanged chains for A_2B_3 micelle solutions with $\varphi = 0.02$–0.05, $a_{AB} = 50$), the overall chain exchange kinetics follow first order kinetics with a single relaxation time.

Comparing the results obtained for A_2B_3 micelle solutions at different polymer concentrations, we found that chain exchange

process (Fig. 2, inset) is independent of concentration and is dominated by unimer (small aggregate) expulsion. Unimer insertion, which occurs more rapidly for micelle solutions with higher oligomer concentration occurs at a noticeably shorter time scales than chain expulsion and hence does not significantly influence the chain exchange kinetics. At the same time, the correlation function for unimer formation (from chains being originally part of micelles), $E(t)$, eqn (3), shows a strong concentration dependence (Fig. 3)—unimers form more slowly in the micelle solutions with higher oligomer concentration, where the contribution of micelle fusion/fission is higher (Table 3). Since the characteristic time for native chain expulsion from micelles $F(t)$ does not exhibit a concentration dependence, it is the transport of chains between micelles *via* fusion/fission mechanism, which slows down unimer formation, that is responsible for the concentration dependence of $E(t)$.

We also studied the influence of the corona block length on the chain exchange kinetics in A_4B_x micelle solutions and found that chain exchange and native chain expulsion both occur more rapidly for diblock copolymers with longer corona blocks. These results are in contrast to theoretical predictions made in the limit of long chain length[6,7] that chain exchange kinetics slow down with corona block length due to the decrease in the chain diffusion through the corona for longer corona lengths. The decrease in diffusion coefficient in solution with an increase in corona block length does not have an appreciable effect on the observed chain exchange as unimer insertion occurs much quicker than chain expulsion. More importantly for reasonably short diblock copolymers, as considered in our study, the micelle average aggregation number decreases and cmc increases with an increase in corona block length, which implies a higher compatibility with solvent and a somewhat weaker tendency to form micelles compared to a diblock with a shorter corona block (and the same core block). This factor was not considered in the theoretical models for the kinetics of chain exchange between polymer micelles.[6,7] Having a higher cmc and lower cmt for micelles formed by diblock copolymers with longer corona-block length indicates that there is a higher penalty for chain transfer from the bulk to a micelle and therefore a lower potential barrier for a chain escape from the micelle,[13,60] which translates into more rapid chain exchange kinetics.

In summary, using DPD simulations, we studied systematically the influence of the oligomer concentration, interaction energy and corona block length on the chain exchange kinetics between copolymer micelles in solutions. The obtained results provide new insights on the time scales and mechanisms of chain exchange in block copolymer micelle solutions, which will be useful for future development of analytical models and experimental research on polymer self-assembly.

Acknowledgements

We are grateful to Matthew Hagy for his help in the initial development of codes for data analysis. This material is based upon work supported by the National Science Foundation under Grant No. 0348302. All simulations were conducted on the High Performance Computing cluster of Case Western Reserve University.

References

1 G. Riess, *Prog. Polym. Sci.*, 2003, **28**, 1107–1170.
2 J. F. Gohy, *Adv. Polym. Sci.*, 2005, **190**, 65.
3 R. Zana, *Dynamics of Surfactant Self-Assemblies: Micelles, Microemulsions, Vesicles, and Lyotropic Phases*, CRC Press, Boca Raton, FL, USA, 2005.
4 E. Aniansson and S. Wall, *J. Phys. Chem.*, 1974, **78**, 1024–1030.
5 E. Aniansson, S. Wall, M. Almgren, H. Hoffmann, I. Kielmann, W. Ulbricht, R. Zana, J. Lang and C. Tondre, *J. Phys. Chem.*, 1976, **80**, 905–922.
6 A. Halperin and S. Alexander, *Macromolecules*, 1989, **22**, 2403–2412.
7 E. E. Dormidontova, *Macromolecules*, 1999, **32**, 7630–7644.
8 E. Lessner, M. Teubner and M. Kahlweit, *J. Phys. Chem.*, 1981, **85**, 1529–1536.
9 E. Lessner, M. Teubner and M. Kahlweit, *J. Phys. Chem.*, 1981, **85**, 3167–3175.
10 M. Kahlweit, *J. Colloid Interface Sci.*, 1982, **90**, 92–99.
11 L. Willner, A. Poppe, J. Allgaier, M. Monkenbusch, P. Lindner and D. Richter, *Europhys. Lett.*, 2000, **51**, 628–634.
12 I. LaRue, M. Adam, E. B. Zhulina, M. Rubinstein, M. Pitsikalis, N. Hadjichristidis, D. A. Ivanov, R. I. Gearba, D. V. Anokhin and S. S. Sheiko, *Macromolecules*, 2008, **41**, 6555–6563.
13 L. Cantu, M. Corti and P. Salina, *J. Phys. Chem.*, 1991, **95**, 5981–5983.
14 K. Prochazka, B. Bednar, E. Mukhtar, P. Svoboda, J. Trnena and M. Almgren, *J. Phys. Chem.*, 1991, **95**, 4563–4568.
15 Y. Wang, R. Balaji, R. P. Quirk and W. L. Mattice, *Polym. Bull.*, 1992, **28**, 333–338.
16 M. Tian, A. Qin, C. Ramireddy, S. E. Webber, P. Munk, Z. Tuzar and K. Prochazka, *Langmuir*, 1993, **9**, 1741–1748.
17 Y. Wang, C. M. Kausch, M. Chun, R. P. Quirk and W. L. Mattice, *Macromolecules*, 1995, **28**, 904–911.
18 S. Creutz, J. Van Stam, S. Antoun, F. C. De Schryver and R. Jerome, *Macromolecules*, 1997, **30**, 4078–4083.
19 R. S. Underhill, J. Ding, V. I. Birss and G. Liu, *Macromolecules*, 1997, **30**, 8298–8303.
20 S. Creutz, J. Van Stam, F. C. De Schryver and R. Jerome, *Macromolecules*, 1998, **31**, 681–689.
21 F. Esselink, E. Dormidontova and G. Hadziioannou, *Macromolecules*, 1998, **31**, 2925–2932.
22 F. Esselink, E. Dormidontova and G. Hadziioannou, *Macromolecules*, 1998, **31**, 4873–4878.
23 Y. Rharbi, M. Li, M. A. Winnik and K. G. Hahn,Jr, *J. Am. Chem. Soc.*, 2000, **122**, 6242–6251.
24 J. Van Stam, S. Creutz, F. C. De Schryver and R. Jerome, *Macromolecules*, 2000, **33**, 6388–6395.
25 L. Willner, A. Poppe, J. Allgaier, M. Monkenbusch and D. Richter, *Europhys. Lett.*, 2001, **55**, 667–673.
26 Y. Y. Won, H. T. Davis and F. S. Bates, *Macromolecules*, 2003, **36**, 953–955.
27 P. Cai, C. Wang, J. Ye, Z. Xie and C. Wu, *Macromolecules*, 2004, **37**, 3438–3443.
28 Š. Popelka, L. Machová, F. Rypáček, M. Špírková, M. Štěpánek, P. Matějíček and K. Procházka, *Collect. Czech. Chem. Commun.*, 2005, **70**, 1811–1828.
29 R. Lund, L. Willner, D. Richter and E. E. Dormidontova, *Macromolecules*, 2006, **39**, 4566–4575.
30 R. Lund, L. Willner, J. Stellbrink, P. Lindner and D. Richter, *Phys. Rev. Lett.*, 2006, **96**, 68302.
31 S. H. Choi, T. P. Lodge and F. S. Bates, *Phys. Rev. Lett.*, 2010, **104**, 047802.
32 M. Hilczer, A. Barzykin and M. Tachiya, *Langmuir*, 2001, **17**, 4196–4201.
33 T. Haliloglu and W. L. Mattice, *Chem. Eng. Sci.*, 1994, **49**, 2851–2857.
34 T. Haliloglu and W. L. Mattice, *Comput. Polym. Sci.*, 1995, **5**, 65–65.
35 T. Haliloglu, I. Bahar, B. Erman and W. L. Mattice, *Macromolecules*, 1996, **29**, 4764–4771.
36 F. K. von Gottberg, K. A. Smith and T. A. Hatton, *J. Chem. Phys.*, 1998, **108**, 2232.
37 M. Pepin and M. Whitmore, *Macromolecules*, 2000, **33**, 8644–8653.
38 P. J. Hoogerbrugge and J. M. V. Koelman, *Europhys. Lett.*, 1992, **19**, 155–160.
39 R. D. Groot and P. B. Warren, *J. Chem. Phys.*, 1997, **107**, 4423.
40 A. Schlijper, P. Hoogerbrugge and C. Manke, *J. Rheol. (N. Y.)*, 1995, **39**, 567.

41 N. Spenley, *Europhys. Lett.*, 2000, **49**, 534–540.
42 W. Jiang, J. Huang, Y. Wang and M. Laradji, *J. Chem. Phys.*, 2007, **126**, 044901.
43 S. Jury, P. Bladon, M. Cates, S. Krishna, M. Hagen, N. Ruddock and P. Warren, *Phys. Chem. Chem. Phys.*, 1999, **1**, 2051–2056.
44 S. Yamamoto, Y. Maruyama and S. Hyodo, *J. Chem. Phys.*, 2002, **116**, 5842.
45 Y. J. Sheng, T. Y. Wang, W. M. Chen and H. K. Tsao, *J. Phys. Chem. B*, 2007, **111**, 10938–10945.
46 Z. Li and E. E. Dormidontova, *Macromolecules*, 2010, **43**, 3521–3531.
47 M. Allen and D. Tildesley, *Computer Simulation of Liquids*, Oxford University Press, USA, 1990.
48 S. Plimpton, *J. Comput. Phys.*, 1995, **117**, 1–19.
49 S. Marrink, D. Tieleman and A. Mark, *J. Phys. Chem. B*, 2000, **104**, 12165–12173.
50 W. Humphrey, A. Dalke and K. Schulten, *J. Mol. Graphics*, 1996, **14**, 33–38.
51 J. L. Barrat and G. H. Fredrickson, *Macromolecules*, 1991, **24**, 6378–6383.
52 H. Yokoyama and E. J. Kramer, *Macromolecules*, 1998, **31**, 7871–7876.
53 E. B. Zhulina, M. Adam, I. LaRue, S. S. Sheiko and M. Rubinstein, *Macromolecules*, 2005, **38**, 5330–5351.
54 R. Nagarajan and K. Ganesh, *J. Chem. Phys.*, 1989, **90**, 5843.
55 M. D. Whitmore and J. Noolandi, *Macromolecules*, 1985, **18**, 657–665.
56 D. Stauffer and D. Woermann, *J. Phys. II*, 1995, **5**, 1–3.
57 D. F. Anghel, F. M. Winnik and N. Galatanu, *Colloids Surf., A*, 1999, **149**, 339–345.
58 M. Kenward and M. Whitmore, *J. Chem. Phys.*, 2002, **116**, 3455.
59 A. Khan, G. F. Durrani, M. Usman, W. Harrison and M. Siddiq, *J. Chem. Soc. Pak.*, 2010, **31**, 534–542.
60 R. Nagarajan and E. Ruckenstein, *J. Colloid Interface Sci.*, 1983, **91**, 500–506.

